Targeted ubiquitination of sensory neuron calcium channels reduces the development of neuropathic pain

Linlin Sun[a,1,2] , Chi-Kun Tong[b,1] , Travis J. Morgenstern[c,1] , Hang Zhou[a] , Guang Yang[a,3] , and Henry M. Colecraft[b,c,3]

Neuropathic pain caused by lesions to somatosensory neurons due to injury or disease is a widespread public health problem that is inadequately managed by small-molecule therapeutics due to incomplete pain relief and devastating side effects. Genetically encoded molecules capable of interrupting nociception have the potential to confer long-lasting analgesia with minimal off-target effects. Here, we utilize a targeted ubiquitination approach to achieve a unique posttranslational functional knockdown of high-voltage-activated calcium channels (HVACCs) that are obligatory for neurotransmission in dorsal root ganglion (DRG) neurons. Ca_V-aβlator comprises a nanobody targeted to Ca_V channel cytosolic auxiliary β subunits fused to the catalytic HECT domain of the Nedd4-2 E3 ubiquitin ligase. Subcutaneous injection of adeno-associated virus serotype 9 encoding Ca_V-aβlator in the hind paw of mice resulted in the expression of the protein in a subset of DRG neurons that displayed a concomitant ablation of Ca_V currents and also led to an increase in the frequency of spontaneous inhibitory postsynaptic currents in the dorsal horn of the spinal cord. Mice subjected to spare nerve injury displayed a characteristic long-lasting mechanical, thermal, and cold hyperalgesia underlain by a dramatic increase in coordinated phasic firing of DRG neurons as reported by *in vivo* Ca^{2+} spike recordings. Ca_V-aβlator significantly dampened the integrated Ca^{2+} spike activity and the hyperalgesia in response to nerve injury. The results advance the principle of targeting HVACCs as a gene therapy for neuropathic pain and demonstrate the therapeutic potential of posttranslational functional knockdown of ion channels achieved by exploiting the ubiquitin-proteasome system.

calcium channel | ubiquitin | neuropathic pain

Neuropathic pain is a debilitating ailment caused by lesions in the somatosensory system that can arise from diverse conditions including nerve injuries, diabetes, thoracic surgery, cancer, and chemotherapy-induced neuropathy. The condition is widely prevalent, affecting ~10% of the general population and is the most difficult type of chronic pain to treat (1, 2). First-line treatments for neuropathic pain commonly include gabapentinoids (gabapentin or pregabalin) or antidepressants, with opioid agonists such as tramadol frequently prescribed as second-line treatments (3–5). Unfortunately, up to 40% of patients remain refractory to these treatments, and serious side effects of these medications further limit their clinical utility. For example, gabapentin only reduces chronic neuropathic pain by at least 50% in fewer than 20% of patients (6), and pregabalin is not effective in controlling chronic pain after traumatic nerve injury (7). Adverse side effects of gabapentinoids due to central actions include sedation, dizziness, drowsiness, fatigue, and blurred vision (8, 9). Opiate agonists also have well-recognized limitations—dose-limiting adverse effects, inadequate pain relief, requirement for multiple daily dosing, liver/kidney toxicity, high potential for abuse and addiction, and risk of overdose—that largely reduce their efficacy for treating neuropathic pain (10). Overall, neuropathic pain is a significant public health problem lacking adequate therapeutic options. As such, there is a salient need to develop treatment modalities that provide strong, long-lasting, and nonaddictive pain relief, with few side effects.

Gene therapy has emerged as an attractive alternative approach to treat chronic pain, with the notion that sustained but locally restricted expression of a therapeutic transgene can potentially enable long-lasting alleviation of nociception after a single dose, with minimal side effects (11, 12). A critical decision is the choice of the gene or protein to be targeted and its role in the pain processing pathway. High-voltage-activated calcium channels (HVACCs) are attractive potential targets for a gene therapy approach because 1) presynaptic Ca_V2 channels in nociceptive somatosensory neurons mediate the central release of a neurotransmitter in the dorsal horn of the spinal cord, which is an obligatory step in nociception, and 2) several analgesics including gabapentinoids (13, 14), ziconotide (15), and opiate agonists acting on μ-opioid receptors to release $G_{\beta\gamma}$ subunits (16) inhibit Ca_V2 channels as a mechanism for alleviating pain.

Significance

Neuropathic pain affects nearly 10% of the US population, and yet current treatments with small-molecule drugs fail to adequately alleviate nociception and often produce serious side effects. High-voltage-activated calcium channels (HVACCs) are membrane proteins that are necessary for synaptic transmission in sensory neurons, and inhibiting these channels is a proven method to achieve analgesia. In this work, we used subcutaneous injection to express a genetically encoded molecule that blocks HVACCs in sensory neurons in vivo. We demonstrate that this approach effectively reduces the onset of neuropathic pain in an animal model of the disease without any observable side effects. These studies support the development of a gene therapy targeting the inhibition of HVACCs to preempt, and potentially reverse, neuropathic pain.

[1]L.S., C.-K.T., and T.J.M. contributed equally to this work.

[2]Present address: Neuroscience Research Institute, Peking University, Beijing 100191, China.

[3]To whom correspondence may be addressed. Email: hc2405@cumc.columbia.edu or gy2268@cumc.columbia.edu.

Thus, we hypothesized that targeted down-regulation of HVACCs in somatosensory neurons in vivo would be efficacious as a long-lasting treatment for neuropathic pain. Previous studies seeking to downregulate the expression of proteins involved in nociception have used RNA interference or antisense approaches (17, 18). More recently, epigenetic suppression of Nav1.7 in mice was achieved using catalytically dead CRISPR-Cas9 and zinc finger protein approaches, respectively, to achieve analgesia in rodent models (19). By comparison with these methods, posttranslational knockdown of relevant proteins offers an alternative approach with potential advantages that include quicker onset of pain relief, easier titration of effects, and fewer obstacles to clinical development.

We recently developed a genetically encoded potent HVACC blocker comprised of an auxiliary $Ca_V\beta$-subunit-targeted nanobody (nb.F3) fused to the catalytic HECT domain of the E3 ubiquitin ligase Nedd4L (neural precursor cell expressed developmentally downregulated gene 4-like) (20). Here, we investigated whether the expression of nb.F3-Nedd4L$_{HECT}$ (also known as Ca_V-aβlator) in sensory neurons in mice is able to inhibit Ca_V channels in vivo and result in the alleviation of experimentally induced nocifensive responses. We show that Ca_V-aβlator can be targeted to sensory neurons via hind paw injection of adeno-associated virus serotype 9 (AAV9) in vivo. The expressed Ca_V-aβlator posttranslationally inhibits HVACCs in DRG neurons, results in increased spontaneous inhibitory postsynaptic currents (sIPSCs) in the spinal cord dorsal horn, and reduces the development of nocifensive responses following nerve injury with no apparent adverse effects. The results not only provide a paradigm of genetically encoded calcium channel blocker development and use for pre-emptive analgesia but also demonstrate the efficacy of harnessing a ubiquitin-dependent posttranslational knockdown approach to achieve treatment of chronic pain.

Results

AAV9-Mediated In Vivo Expression of Ca_V-aβlator in Sensory Neurons Inhibits HVACCs. Chronic neuropathic pain is initiated by lesions to pseudounipolar somatosensory primary afferent neurons that have cell bodies in dorsal root ganglion (DRG) and two axonal branches that innervate peripheral tissues/organs and terminate centrally in the spinal cord, respectively (Fig. 1) (21, 22). In neuropathic pain, injured nerves and nonneuronal cells such as glia and mast cells release factors (e.g., substance P, CGRP, bradykinin) that cause uninjured nearby neurons to undergo neurophysiological and neurochemical changes that increase their intrinsic excitability and expression of pain-associated molecules (23). Signal integration occurs in the spinal cord and involves complex circuits and cell types including numerous excitatory (glutamatergic) and inhibitory (GABAergic and glycinergic) interneurons and descending inhibitory inputs (24, 25). Projection neurons relay signals from the spinal cord to various regions of the brain that mediate the perception of the sensory-discriminative and affective-motivational dimensions of pain (21). Previous gene therapy approaches have included the knockdown of Nav1.7 (using either antisense or CRISPR dCas9-mediated epigenetic knockdown), small interfering RNA (siRNA)-mediated knockdown of postsynaptic NMDA receptors, overexpression of glutamate decarboxylase to catalyze production of GABA, and overexpression of preproenkephalin to act on μ-opioid receptors to inhibit presynaptic Ca_V channels (and activate GIRK channels) via released Gβγ subunits (Fig. 1). A gene therapy approach that directly inhibits or eliminates HVACCs in nociceptive neurons would be expected to be particularly effective for neuropathic pain given the obligatory role of principally Ca_V2 channels in synaptic transmission. However, this has not been previously achieved. Moreover, a posttranslational mechanism of channel inhibition could have advantages over RNA interference or epigenetic approaches related to a quicker onset of pain relief, easier capacity to titrate effects, and fewer obstacles to clinical development. Nevertheless, such posttranslational knockdown of proteins for gene therapy of nociception has not been previously demonstrated.

We previously reported a genetically encoded molecule comprised of a $Ca_V\beta$-targeted nanobody (nb.F3 that binds all four $Ca_V\beta$ subunits, namely, β_1 to β_4) fused to the catalytic HECT domain of the E3 ubiquitin ligase Nedd4L. This molecule, termed Ca_V-aβlator, potently eliminates all types of HVACC currents (I_{Ca}) by promoting the internalization of Ca_V1/Ca_V2 channels (20). Given the indispensable role of HVACCs in conveying pain signals from the periphery to the brain, we sought to test whether Ca_V-aβlator expressed in sensory neurons in vivo would effectively inhibit I_{Ca} and yield a therapeutic benefit in an animal model of neuropathic pain.

We incorporated Ca_V-aβlator into an AAV9 and first injected it subcutaneously into the hind paw of newborn (3 to 5 d old) *Thy1*-GCaMP6s mice that express the genetically encoded Ca^{2+} indicator GCaMP6s in excitatory neurons (Fig. 2 A and B). We used tdTomato as a fluorescent marker of Ca_V-aβlator expression using a P2A construct in which both proteins are separately expressed from a single mRNA. Four weeks after AAV9 injection, we acutely isolated and cultured DRG neurons and imaged the cells for tdTomato and GCaMP6s fluorescence by confocal microscopy. We found that many, but not all, GCaMP6s-positive cells also expressed robust tdTomato fluorescence, confirming that subcutaneous injection of AAV9 successfully infects a population of DRG neurons (Fig. 2B). We used whole-cell patch clamp to examine the impact of Ca_V-aβlator on I_{Ca} in DRG neurons, using 5 μM mibefradil in the bath to suppress T-type calcium channels. tdTomato-negative cells yielded large whole-cell Ca^{2+} currents that were completely eliminated in neurons expressing Ca_V-aβlator (tdTomato-positive cells) (Fig. 2C).

We next examined whether AAV9-mediated delivery of Ca_V-aβlator in adult mice could also yield significant infection of sensory neurons in vivo. We subcutaneously injected 7.2×10^{11} vg of AAV9 encoding pFB-CMV-tdTomato-P2A-F3-Nedd4L (Ca_V-aβlator) into the left hind paw of 6- to 8-wk-old C57BL mice (Fig. 2D). Four to 6 weeks following AAV injection, the mice were euthanized and their sciatic nerves, lumbar dorsal roots, DRGs, and ventral skin of the injected paw were collected, fixed, cryosectioned, and imaged using confocal microscopy. In control experiments with uninjected wild-type mice, we observed significant autofluorescence of the cryo-sectioned tissue in the red channel that would complicate our ability to observe tdTomato fluorescence in injected mice due to signal overlap. Many microstructures, including blood vessels and cell organelles, such as mitochondria, lysosome, and lipofuscin, are known to display autofluorescence by confocal microscopy (26–29). To distinguish true tdTomato fluorescence from autofluorescence, we exploited the fact that autofluorescence emitted by the organelles can be seen in both red and green channels, thus enabling the green autofluorescence to be used for a "background" subtraction of red fluorescence signals. Using this approach, we observed bright tdTomato fluorescence in some DRG neurons, sciatic nerves, and dorsal roots from AAV9-injected injected mice (Fig. 2E and *SI Appendix*, Fig. S1), while no expression was observed in the skin
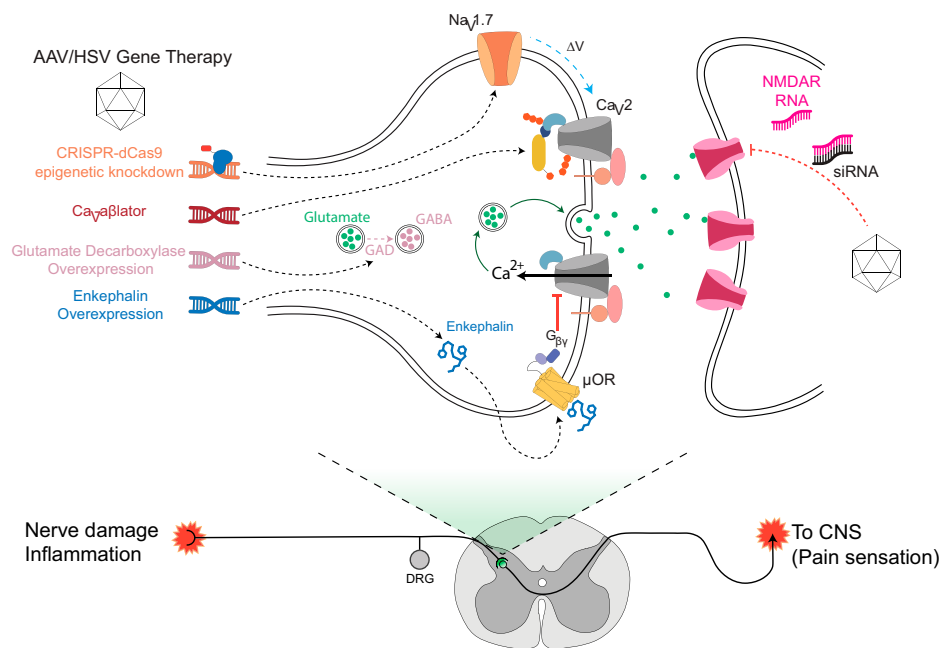
Fig. 1. Distinct paradigms and targets for neuropathic pain gene therapy. The circuitry for neuropathic pain involves signals from primary somatosensory neurons that synapse on secondary neurons in the spinal cord dorsal horn. Relay neurons convey signals to various parts of the brain for nociception. Key signaling molecules and proteins involved in the relaying of nociceptive signals are candidate targets for neuropathic pain gene therapy. Previously described knockdown approaches include CRISPR-dCas9-mediated epigenetic knockdown of Nav1.7 and down-regulation of NMDA receptors with siRNA. Overexpression of glutamate decarboxylase has been used to produce the inhibitory neurotransmitter GABA; enkephalin overexpression suppresses neurotransmission by activating the μ-opioid receptor to release $G_{\beta\gamma}$ subunits that inhibit presynaptic $Ca_V2.2$ channels. Ca^{2+} influx through Ca_V2 channels is necessary for neurotransmitter release, and inhibiting these channels is therapeutic for chronic pain. Here, we use a targeted ubiquitination strategy to achieve direct posttranslational functional knockdown of Ca_V2 channels in DRG neurons using Ca_V-aβlator, a genetically encoded molecule featuring a $Ca_V\beta$-targeted nanobody fused to the catalytic HECT domain of Nedd4 E3 ligase. μOR, μ-opioid receptors.

tissues of the injected hind paw. Thus, Ca_V-aβlator was successfully expressed in a subpopulation of primary afferent fibers and DRG neurons when delivered to adult mice by subcutaneous AAV9 injection in the hind paw. The level of Ca_V-aβlator expression observed in tissue sections from adult mice appeared relatively modest compared to that seen following injection in newborn mice. Nevertheless, similar to what we observed in young mice, DRG neurons isolated from injected adult mice and expressing Ca_V-aβlator (as indicated by tdTomato fluorescence) displayed markedly smaller whole-cell I_{Ca} ($I_{Ca,max} = -9.1 \pm 3.2$ pA/pF, $n = 10$ from $n = 2$ mice) than tdTomato-negative neurons isolated from the same animals ($I_{Ca,max} = -77.7 \pm 17.8$ pA/pF, $n = 19$) (Fig. 2F). To ensure that tdTomato expression itself did not downregulate calcium channels, we also tested the functional impact of a control AAV9 encoding tdTomato alone. Four weeks following injection of 20 μL control tdTomato AAV9 in a 10-wk-old mouse, a whole-cell patch clamp of isolated cultured DRG neurons showed that both tdTomato-positive and tdTomato-negative neurons displayed similar HVACC currents ($I_{Ca,max} = -73.4 \pm 21.9$ pA/pF, $n = 5$, for tdTomato-positive neurons, and $I_{Ca,max} = -75.6 \pm 25.2$ pA/pF, $n = 6$) (*SI Appendix*, Fig. S2).

Ca_V-aβlator Expression in DRG Neurons Increases the Frequency of sIPSCs in Dorsal Horn Neurons in the Spinal Cord. We wondered whether the level of expression of Ca_V-aβlator in sensory neurons achieved following hind paw injection of AAV9 was sufficient to induce a measurable change in the electrophysiological signature of dorsal horn neurons in the spinal cord. Accordingly, we compared synaptic activity in the dorsal horn of the Ca_V-aβlator-injected side with control side using whole-cell patch clamp recording in the superficial dorsal horn lamina I and II, which is an area that predominantly

receives input from small unmyelinated and lightly myelinated primary afferents and is critical for nociception (25).

Wild-type 6- to 8-wk-old C57BL mice were injected with Ca_V-aβlator AAV9 into the left hind paws. Spinal cord slices were collected 4 to 5 weeks following the injection for electrophysiology recordings. We did not observe any significant difference in either the amplitude of spontaneous excitatory postsynaptic current (sEPSC) (median = 14.8 pA, range = 12.8 to 23.0 pA, $n = 18$; and median = 14.3 pA, range = 12.8 to 16.0 pA, $n = 13$, for contralateral control and Ca_V-aβlator-injected sides, respectively) or their frequency (median = 20.0 min^{-1}, range = 4.4 to 30.3 min^{-1}, $n = 18$; and median = 21 min^{-1}, range = 9.3 to 48.8 min^{-1}, $n = 13$, for contralateral control and Ca_V-aβlator-injected sides, respectively) (Fig. 3 A–D).

We next examined a potential impact of Ca_V-aβlator expression on sIPSCs. We observed no significant difference in sIPSC amplitude between the Ca_V-aβlator-injected side and the contralateral control (median = 16.1 pA, range = 11.2 to 20.0 pA, $n = 21$ for control; and median = 16.0 pA, range = 12.8 to 18.6 pA, $n = 18$ for Ca_V-aβlator-injected sides) (Fig. 3 E–H). By contrast, we found that the frequency of sIPSCs was significantly higher in the dorsal horn of the high Ca_V-aβlator-injected side than that of the contralateral control group (median = 28 min^{-1}, range = 13.5 to 53.5 min^{-1}, $n = 18$ for Ca_V-aβlator-injected side; and median = 11.5 min^{-1}, range = 2.8 to 26.3 min^{-1}, $n = 21$ for contralateral control, $P = 0.031$ unpaired t test) (Fig. 3H). Altogether, these data indicate that the level of Ca_V-aβlator expression in sensory neurons after hind paw injection of AAV9 is sufficient to result in a measurable electrophysiological change in the spinal cord, i.e., an apparent increase in the inhibitory input onto dorsal horn neurons.

It is known that GABA and glycine corelease from inhibitory interneurons to activate GABA and glycine receptors, respectively,
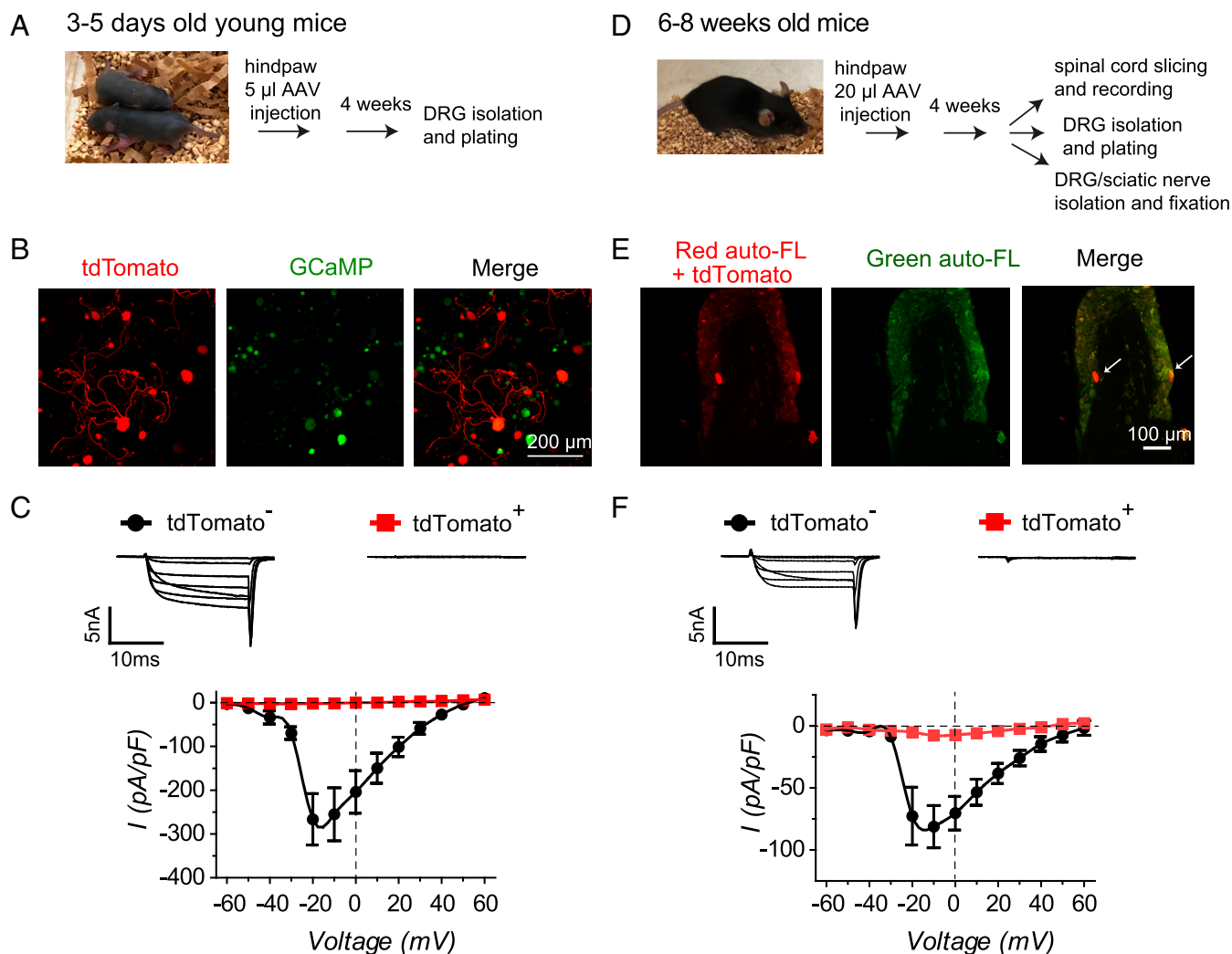
Fig. 2. Ca$_V$-aβlator expressed in vivo ablates calcium currents in DRG neurons. (*A*) Experimental paradigm for Ca$_V$-aβlator injection in newborn mice. (*B*) Confocal images of cultured DRG neurons from Thy1-GCaMP6s mouse injected at 3 to 5 d old in the hind paw with AAV9-expressing Ca$_V$-aβlator-P2A-tdTomato. (*C*) *Top*, exemplar family of whole-cell Ca^{2+} channel currents obtained from young mice DRG neurons either negative (tdTomato$^-$) or positive (tdTomato$^+$) for Ca$_V$-aβlator expression. *Bottom*, population Ca^{2+} current *I-V* curves from young mice DRG neurons negative (●, $n = 6$) or positive (red square, $n = 5$) for Ca$_V$-aβlator expression. (*D*) Experimental paradigm for Ca$_V$-aβlator subcutaneous injection in adult mice. (*E*) Confocal image of DRG from a Ca$_V$-aβlator-injected mouse. Autofluorescence in the green channel was exploited to isolate red signals due to Ca$_V$-aβlator-P2a-tdTomato expression from background red autofluorescence. (*F*) *Top*, exemplar family of whole-cell Ca^{2+} channel currents obtained from adult mice DRG neurons either negative (tdTomato$^-$) or positive (tdTomato$^+$) for Ca$_V$-aβlator expression. *Bottom*, population Ca^{2+} current *I-V* curves from adult mice DRG neurons negative (●, $n = 19$) or positive (red square, $n = 10$) for Ca$_V$-aβlator expression.

of individual neurons within the superficial dorsal horn. However, the ratio of GABAergic and glycinergic input to a specific neuron can be changed, for example, by inflammation that triggers a switch from glycine to GABA-receptor-dominant neurons (30). To distinguish whether the enhanced inhibitory input onto the dorsal horn neurons was specifically due to either increased GABAergic or glycinergic activity, we analyzed the decay time constant (τ_{decay}) of the sIPSCs. GABA receptors have a higher τ_{decay} than glycine receptors. Accordingly, the amplitude of τ_{decay} of the sIPSCs of a specific neuron is a good indicator of the type of synapse the neurons receive (31). Following AAV9-Ca$_V$-aβlator injection, we found no change in the sIPSC τ_{decay} amplitude between contralateral control and Ca$_V$-aβlator-treated sides (median = 8 ms, range 4.3 to 13.5 ms, $n = 19$ for control; and median = 8.2 ms, range = 7.1 to 16.4 ms, $n = 13$ for Ca$_V$-aβlator-injected side, $P = 0.65$) (*SI Appendix*, Fig. S3), suggesting that the increased inhibition onto dorsal horn neurons is not restricted to either GABAergic or glycinergic inputs.

Ca$_V$-aβlator Expression In Vivo Reduces the Nerve-Injury-Mediated Increase in DRG Neuron Excitability and Development of Nocifensive Responses. We recently developed an approach that enables long-term imaging of Ca^{2+} signals in DRG neurons in awake behaving mice (32). Using this approach, we demonstrated that formalin-induced inflammatory pain is correlated with increased phasic and persistent hyperactivity of nociceptive DRG neurons in vivo. We sought to determine whether Ca$_V$-aβlator administered by AAV9 injection in the hind paw could suppress the anticipated DRG neuron hyperactivity in a nerve injury model of chronic pain. Here, we injected adult *Thy1*-GCaMP6s mice subcutaneously in the left hind paw with AAV9-encoding tdTomato-P2A-Ca$_V$-aβlator under the CMV promoter (Fig. 4*A*). The vehicle control mice were injected with AAV9-encoding tdTomato without Ca$_V$-aβlator. Three weeks later, an intervertebral fusion mount was combined with implantation of a vertebral glass window to enable in vivo imaging of DRG neuron activity in awake mice. Four weeks after AAV injection, the spared nerve
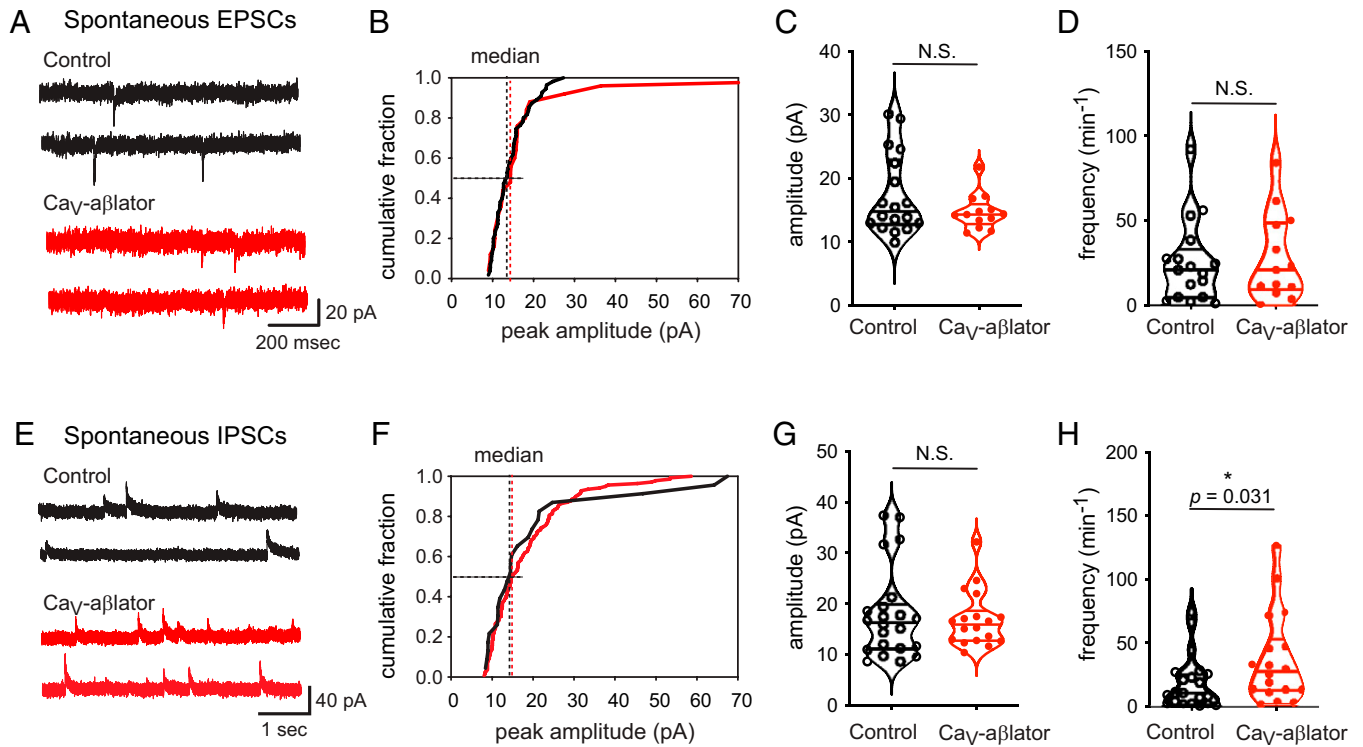
Fig. 3. Impact of Ca$_V$-aβlator expression in DRG neurons on spontaneous EPSCs and IPSCs in the spinal cord dorsal horn. (*A*) Exemplar sEPSC recorded in the dorsal horn from control (black traces) and Ca$_V$-aβlator-injected (red traces) sides. (*B*) Cumulative distribution histograms of exemplar sEPSC amplitudes for control (black line) and Ca$_V$-aβlator-injected (red line) sides. (*C*) Population mean sEPSC amplitudes from control and Ca$_V$-aβlator-injected sides. (*D*) Summary of sEPSC frequency. N.S., not significant. (*E*) Exemplar sIPSC recorded in the dorsal horn from control (black traces) and Ca$_V$-aβlator-injected (red traces) sides. (*F*) Cumulative distribution histograms of exemplar sIPSC amplitudes for control (black line) and Ca$_V$-aβlator-injected (red line) sides. (*G*) Population mean sIPSC amplitudes from control and Ca$_V$-aβlator-injected sides. (*H*) Summary of sIPSC frequency.

injury (SNI) model of neuropathic pain was initiated by ligating two branches of the sciatic nerve, the tibial and common peroneal nerves, while sparing the sural nerve.

In control mice (SNI + tdTomato), in vivo Ca^{2+} imaging of DRG neurons using two-photon microscopy showed low-amplitude Ca^{2+} signals that were uncoordinated among different cells, reflecting basal neuronal activity pre-SNI (Fig. 4*B*). Three days after SNI, control DRG neurons displayed an increase in spontaneous activity in vivo characterized by moderate increases in the frequency, mean peak amplitude, and synchronicity of Ca^{2+} transients (Fig. 4 *B*, *D*, and *E*). Seven days post-SNI, there was a dramatic increase in the frequency (2.01 ± 0.14 spikes/min pre-SNI vs. 5.99 ± 0.21 spikes/min 7 d post-SNI), mean amplitude (ΔF/F_0 = 0.37 ± 0.02 pre-SNI vs. 1.53 ± 0.18 7 d post-SNI), and synchronicity of Ca^{2+} transients in control mice DRG neurons (Fig. 4 *B*, *D*, and *E*). Overall, the integrated Ca^{2+} activity in DRG neurons increased over fourfold in vivo between pre-SNI and 7 d post-SNI (Fig. 4*F*). The increase in neuronal Ca^{2+} activity post-SNI is in agreement with our previous observation that plantar formalin injection that produces inflammatory nociception in mice induces a long-lasting augmentation of Ca^{2+} transients in DRG neurons in vivo (32). The results are also consistent with the phenomenon of peripheral sensitization known to occur in neuropathic pain. In isochronal test animals injected with Ca$_V$-aβlator AAV9, there was also an increase in the frequency, mean amplitude, and integrated Ca^{2+} activity between pre- and post-SNI conditions (Fig. 4 *C*–*G*). However, the increase in Ca^{2+} signals and activity synchrony observed in Ca$_V$-aβlator-injected mice was significantly lower than that observed in control mice (Fig. 4 *B*–*G*).

In accord with the observed increase in DRG neuron excitability, control mice displayed a long-lasting mechanical allodynia as indicated by a reduced paw withdrawal threshold (PWT) in the von Frey test that was evident 3 d after SNI and persisted after 7 d of observation (Fig. 5*A*). In the test, mice of both sexes were injected with Ca$_V$-aβlator, and there was a significant reduction in mechanical allodynia that persisted over 7 d (Fig. 5*A*). Beyond mechanical allodynia, control mice injected with AAV9-tdTomato vehicle also displayed a persistent increased sensitivity to thermal and cold stimuli as reported by a reduced paw withdrawal latency after SNI. Mice injected with Ca$_V$-aβlator AAV9 showed significantly less thermal and cold sensitivity after SNI than contemporaneous vehicle-injected controls (Fig. 5*A*). One concern was that Ca$_V$-aβlator could potentially be expressed in unintended tissues and cells and lead to adverse off-target effects. We conducted a series of behavioral tests to evaluate the prevalence of potential inimical consequences of in vivo Ca$_V$-aβlator expression. We observed no difference between vehicle and Ca$_V$-aβlator-AAV9-injected mice in open field (Fig. 5*B*), rotarod (Fig. 5*C*), and locomotor and reflex tests, including placing, grasping, and righting reflexes (Fig. 5*D*).

Discussion

In this study, we utilized a targeted ubiquitination approach with Ca$_V$-aβlator to selectively remove HVACCs from the surface of DRG neurons. When delivered in vivo by AAV9 injection into the hind paw of mice, Ca$_V$-aβlator is expressed in a subset of DRG neurons and 1) strongly inhibits HVACC currents, 2) results in an increase in the frequency of sIPSCs in the spinal cord dorsal horn, 3) dampens the increase in DRG neuron Ca^{2+}
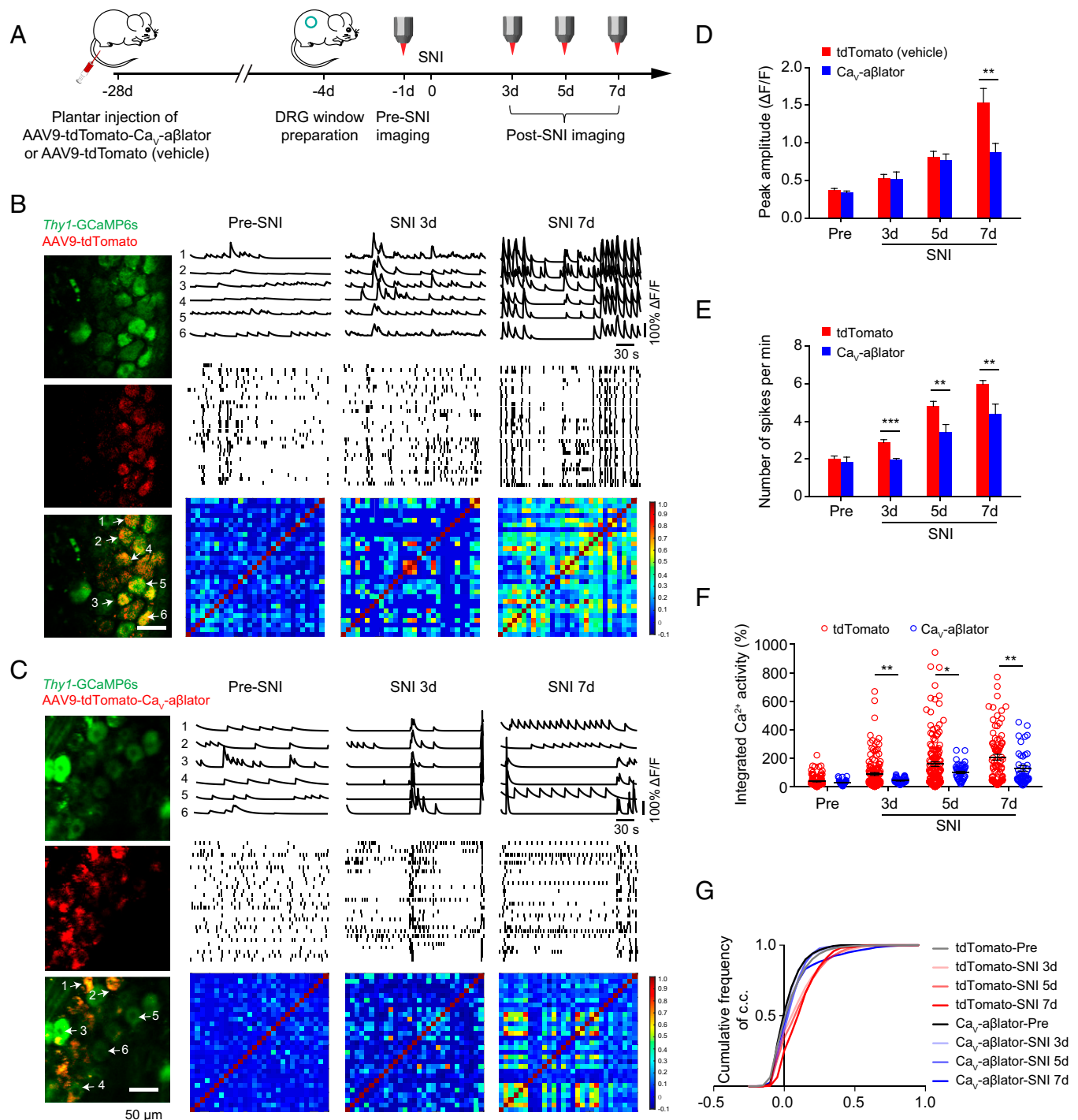
Fig. 4. Impact of Ca_V-aβlator on nerve-injury-induced enhancement of spontaneous calcium spikes in DRG neurons in vivo. (*A*) Experimental design. (*B*) Spontaneous Ca^{2+} spikes recorded in vivo in DRG neurons from a control *Thy1*-GCaMP6s mouse (injected with AAV9-tdTomato) pre-SNI and 3 and 7 d post-SNI. *Left*, images of DRG neurons expressing GCaMP6s and/or tdTomato. *Right*, representative Ca^{2+} traces (*Top*), deconvoluted somatic Ca^{2+} spikes from 30 DRG neurons (*Middle*), and representative correlation coefficient matrix of Ca^{2+} transients from all active neuron pairs in DRG (*Bottom*). Ca^{2+} traces 1 to 6 correspond to individual neurons 1 to 6 indicated by arrows in the DRG image. (*C*) In vivo spontaneous Ca^{2+} transient data for *Thy1*-GCaMP6s mouse injected subcutaneously with AAV9-encoding tdTomato-Ca_V-aβlator, with the same format as *B*. (*D*) Summary of mean peak amplitude of spontaneous Ca^{2+} spikes between tdTomato- and Ca_V-aβlator-injected mice pre- and post-SNI. (*E*) Summary of mean frequency of spontaneous Ca^{2+} spikes. (*F*) Average integrated Ca^{2+} activity of DRG neurons ($n = 140$ neurons in tdTomato group, $n = 52$ neurons in Ca_V-aβlator group). (*G*) Cumulative curve of the correlation coefficients (c.c.) of all active DRG neuron pairs ($n = 140$ neurons in tdTomato group, $n = 52$ neurons in Ca_V-aβlator group). Summary data are presented as mean ± SEM *$P < 0.05$, **$P < 0.01$, ***$P < 0.001$; by unpaired t test.

signaling in vivo that develops following SNI, 4) and provides a long-lasting relief of SNI-induced mechanical allodynia and hypersensitivity to thermal and cold stimuli, without any apparent adverse effects. These results elevate Ca_V-aβlator as a candidate for development as a potential gene therapy for neuropathic pain. We

discuss here the unique aspects of our approach within the broader context of previous studies probing the potential of developing gene therapies for the treatment of chronic pain.

DRG neurons express multiple types of HVACCs including $Ca_V1.2$, $Ca_V2.1$, $Ca_V2.2$, and $Ca_V2.3$. Ca^{2+} influx through

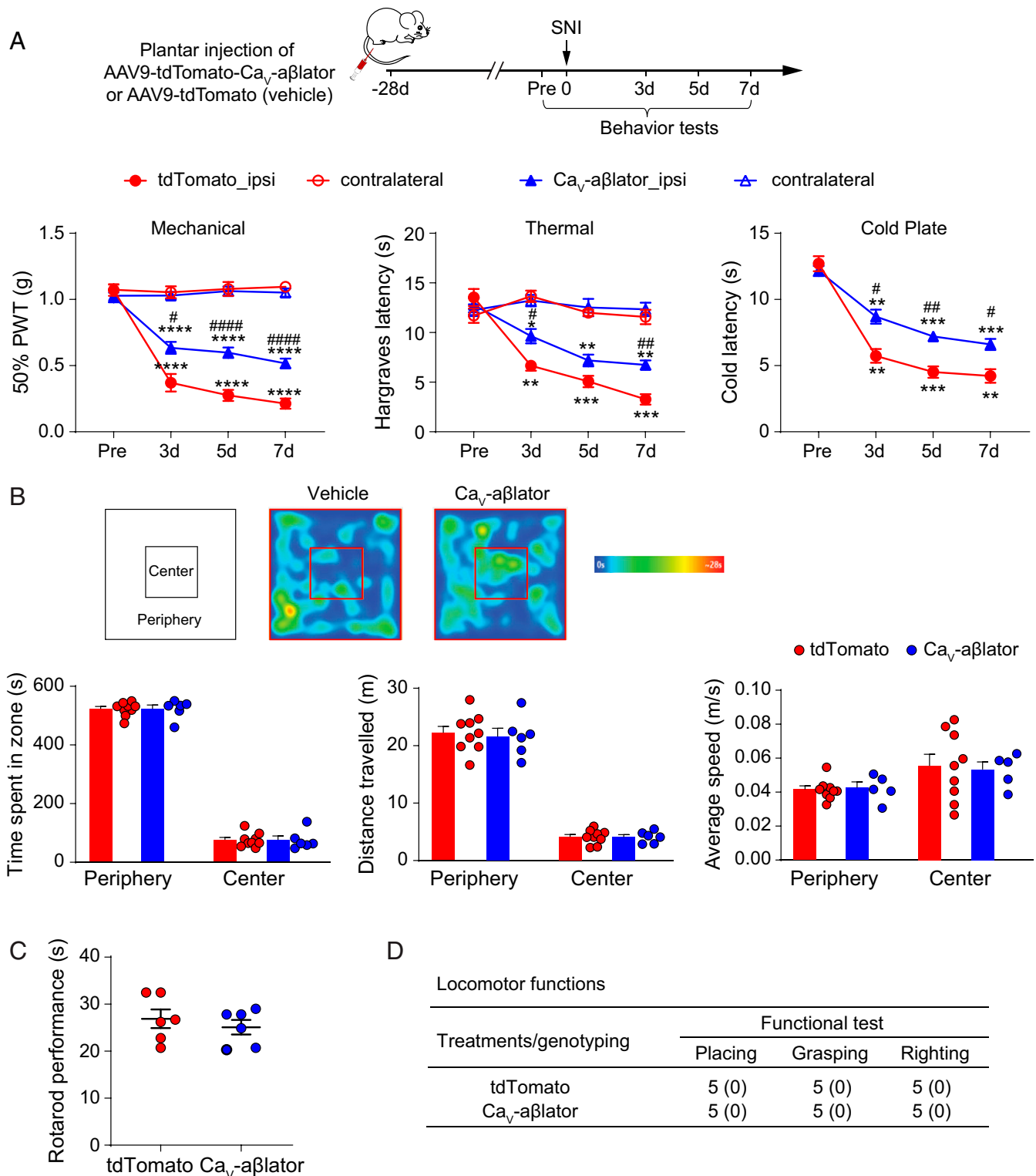**Fig. 5.** Ca$_V$-aβlator reduces hyperalgesia after SNI with no apparent adverse effects. (*A*) *Top*, shows experimental design. Mice were tested 4 weeks after viral injection. *Bottom*, shows behavior tests for nocifensive responses. SNI triggered the development of mechanical, thermal, and cold hypersensitivity in the ipsilateral (ipsi) but not contralateral (contra) side of the mice, and the hypersensitivity was significantly reduced in Ca$_V$-aβlator injected mice. (*n* = 6 to 9 mice per group). (*B*) Open field test showed no difference between tdTomato- and Ca$_V$-aβlator-injected mice. (*C*) Rotarod performance test. Each dots represent data from a single animal. (*D*) Scores for placing, grasping, and righting reflexes were based on counts of each normal reflex exhibited in five trials. All values are mean (SEM). *n* = 6 mice per group. There was no difference in locomotor functions between tdTomato- and Ca$_V$-aβlator-injected mice. Summary data are presented as mean ± SEM *$P < 0.05$, **$P < 0.01$, ***$P < 0.001$, ****$P < 0.0001$; #$P < 0.05$, ##$P < 0.01$, ####$P < 0.0001$; by two-way RM ANOVA with Dunnett's multiple comparisons test (*A*), or unpaired *t* test (*B*, *C*). Asterisks (*) denote post-SNI versus pre-SNI (day 0) comparisons, and the pound signs (#) denote the comparison Ca$_V$-aβlator versus control.

these HVACCs mediates diverse functions in somatosensory neurons including regulating excitability by coupling to Ca^{2+}-activated K$^+$ and Cl$^-$ channels, controlling the release of a neurotransmitter in the spinal cord dorsal horn and coupling excitation to regulation of gene expression. The whole-cell HVACC current in DRG neurons is found to be significantly

downregulated after nerve injury that results in nocifensive responses, with decreases extending to $Ca_V1.2$, $Ca_V2.1$, and $Ca_V2.2$ channels (33–35). The decrease in whole-cell HVACC current likely plays a prominent role in the increased excitability of DRG neurons in chronic pain, as inhibiting HVACCs with a mixture of blockers diminishes outward Ca^{2+}-activated K^+ currents, prolongs nociceptor action potential duration, and reduces amplitude of the afterhyperpolarization potential (AHP) (33). Nevertheless, the conveyance of electrical signals from hyperexcitable somatosensory neurons to central neurons in the dorsal horn in neuropathic pain is still absolutely dependent on Ca^{2+} influx through presynaptic Ca_V2 and, potentially, $Ca_V1.2$ channels. During peripheral nerve injury, expression levels of Ca_V channel $\alpha_2\delta$-1 subunits are elevated in DRG neurons (36–38). Not surprisingly, Ca_V2 channels are important therapeutic targets for pain. The antinociceptive effects of gabapentinoids are mediated through binding to auxiliary Ca_V channel $\alpha_2\delta$-1 and $\alpha_2\delta$-2 subunits (13, 14); ziconotide, a peptide that is used clinically as a second-line treatment for severe chronic pain, acts by blocking pore-forming α_{1B} ($Ca_V2.2$) subunit and preventing neurotransmitter release from nociceptive neurons in the dorsal horn (15, 39); and the analgesic action of opiates involves voltage-dependent inhibition of presynaptic Ca_V2 channels by $G_{\beta\gamma}$ subunits released in response to agonist binding to μ-opioid receptors (16). Despite Ca_V2 inhibition in DRG neurons being a proven therapy for pain, no previous study has explored a gene therapy directly targeting these channels for the alleviation of nocifensive responses. Ca_V2 channels lie downstream of some previous gene therapies for pain strategies including, overexpressing proenkephalin or endomorphin-2 in DRG neurons (40), or downregulating the expression of Nav1.7 channels (17). In comparison to such upstream targets, direct inhibition of HVACCs by Ca_V-aβlator may be more robust in eliminating different types of pain.

Ca_V-aβlator utilizes a $Ca_V\beta$-targeted nanobody fused to the catalytic HECT domain of Nedd4L to achieve targeted ubiquitination of HVACC complexes, resulting in their elimination from the cell surface. Auxiliary $Ca_V\beta$ subunits play a critical role in the surface trafficking and functional maturation of HVACCs (41). As such, molecules that disrupt the interaction between Ca_V channel pore-forming α_1 and auxiliary β subunits have long been sought after as potentially useful Ca_V channel inhibitors. Structure-based virtual screening and medicinal chemistry led to the identification of small molecules capable of disrupting the Ca_V channel α_1/β interaction (42, 43). These compounds inhibited HVACCs in cells at high micromolar concentrations and yielded analgesic responses in rodent nociception models. Nevertheless, such compounds might be expected to have significant off target effects given the prevalence of HVACCs in all excitable cells and the general important role of the α_1/β interaction in functional expression of Ca_V1 and Ca_V2 channels. Moreover, the mechanism of action requires high concentrations of these small compounds to effectively out-compete the low-nanomolar α_1/β interaction. By contrast to these small molecules, Ca_V-aβlator does not act by competitively inhibiting the α_1/β interaction and is genetically encoded, allowing restricted expression in specific cell populations to limit off-target effects.

The work is further distinguished by the use of nanobody-based targeted ubiquitination to achieve functional elimination of a target protein as a potential gene therapy for pain. Previous studies have utilized RNA interference and antisense oligonucleotide approaches to achieve knockdown of gene expression and to validate putative therapeutic targets in pain research.

For example, recombinant AAV-mediated delivery of siRNA to the NMDA receptor in the spinal cord resulted in a 60 to 75% decrease in NR1 mRNA and prevented mechanical allodynia in response to injection of an inflammatory agent to the paw (44). Similarly, herpes simplex virus (HSV)-mediated antisense knockdown of Nav1.7 in DRG neurons prevented the development of inflammatory hyperalgesia in a mouse model (17). Nevertheless, despite the promise of RNA interference methods, their translation into clinical products has been challenging due to hurdles with their delivery, stability, specificity, and propensity for off-target effects (45). The approach of harnessing the physiological ubiquitin-proteasome system to achieve post-translational knockdown of proteins involved in nociception, as we have demonstrated here with Ca_V-aβlator, offers a complementary method to RNA interference that could advance the clinical development of gene therapy for pain.

A perennial challenge of gene therapy for pain and other diseases is the matter of selective and safe delivery of the therapeutic gene or genetically encoded molecule to the relevant tissue or cell population. Several studies have shown the effectiveness of viral gene delivery into DRG neurons via intrathecal (46, 47) or direct intraganglionic (48, 49) injections. However, these methods are invasive that may limit their clinical applications. Here, we show that footpad injection of AAV9-expressing Ca_V-aβlator was effective in dampening hyperalgesia that develops following SNI, even though the numbers of nerve fibers expressing the protein in vivo appeared relatively modest. This suggests that localized viral-mediated therapeutic gene delivery to a site associated with chronic pain may yield an analgesic effect with expression in just a few nerve fibers innervating the region of interest. On the other hand, we observed only a partial analgesic effect with Ca_V-aβlator that may potentially be boosted by optimizing the numbers of neurons expressing the transgene. Future work will seek to address the challenge of maximizing the fraction of neurons expressing Ca_V-aβlator following subcutaneous injection to achieve a near-complete therapeutic effect while limiting confounding off-target effects. A caveat relevant for the preceding point is that the relatively modest number of neurons we observe that express tdTomato reporter fluorescence is likely to represent a lower limit. Owing to the background fluorescence we observe in fixed samples using confocal microscopy, cells expressing a low level of tdTomato fluorescence would not be counted due to poor signal-to-noise ratio. Indeed, two-photon microscopy on live DRG neurons in vivo suggested a significantly higher fraction (~42% in $n = 6$ mice) of cells expressing Ca_V-aβlator (tdTomato fluorescence) after hind paw injection of AAV9 (Fig. 4 B and C). However, because these mice also expressed GCaMP6s, we could not explicitly use the green channel to background subtract possible autofluorescence.

A potential concern was that some of the AAV9 subcutaneously injected into the hind paw could enter the circulation and affect other tissues in the body. This concern is mitigated by our finding of no obvious adverse effects in mice following footpad injection of AAV9-expressing Ca_V-aβlator—the injected mice showed normal mechanical sensitivity and behaved normally in rotarod, open field, locomotor, and reflex tests. The efficacy of Ca_V-aβlator in eliminating nocifensive responses could potentially be enhanced by switching from AAV9 to HSV as the delivery vehicle. HSV is neurotropic and readily taken up by afferent nerve terminals following subcutaneous injection and retrogradely transported to cell bodies in DRG (50). Moreover, a phase I clinical trial showed that delivery of a HSV-expressing human preproenkephalin to patients

with intractable focal pain due to cancer resulted in no serious adverse events (11). Thus, examining whether HSV-mediated delivery can enhance the efficacy of Ca$_V$-aβlator in alleviating nociception while minimizing potential side effects is an important future goal.

Based on our electrophysiology recordings of the dorsal horn neurons in normal mice, sIPSC frequency was enhanced by Ca$_V$-aβlator while sEPSC frequency and amplitude were unchanged. This result was somewhat unexpected but could explain the reduced development of hyperalgesia following nerve injury. The majority of dorsal horn neurons are excitatory neurons, including projection neurons and interneurons (31). Excitatory neurons account for ~70% of the neurons in lamina I and ~75% in lamina II in the mouse dorsal horn (25, 51). In addition, these excitatory neurons receive strong inhibitory input (52) within the superficial dorsal horn, which results in overall reduced nociceptive signals to the brain. According to the gate control theory, reduced inhibitory input onto superficial dorsal horn neurons following injury unveils polysynaptic pathways that were constantly masked and leads to the development of hyperalgesia (53–55). Conversely, enhanced inhibitory input by transplantation of GABAergic neurons in the dorsal horn before injury limits the development of mechanical hypersensitivity (56, 57). This is consistent with our finding that enhanced inhibitory input within the dorsal horn contributes to reduced nociception, suggesting that the central mechanism of the Ca$_V$-aβlator may contribute to the observed diminished hyperalgesia.

Finally, in this study, we only examined the capacity of Ca$_V$-aβlator to pre-emptively alleviate the development of nocifensive responses. This has a potential application for pre-emptive analgesia, an emerging area in preventing postoperative nociception (58) that can be severe in some surgeries, such as thoracic surgery (59, 60). Evaluating the efficacy of Ca$_V$-aβlator to reduce neuropathic pain after it is already established is an important goal for the future.

Methods

Animal Use.
All animal experiments were conducted with approval from and in accordance with policies of the Columbia University Institutional Animal Care and Use Committee. Mice were maintained in a temperature-controlled environment at Columbia University Medical Center with ad libitum access to food and water. Adult C57BL/6 mice of both sexes (8 to 12 wk old) were purchased from Jackson Laboratory. Transgenic Thy1.2-GCaMP6s mice expressing GCaMP6 slow in some DRG neurons have been previously described (61). As no significant differences were observed between male and female mice, data from both sexes were grouped together for analysis.

Ca$_V$-aβlator AAV9 Design and Injection.
Ca$_V$-aβlator (pFB-CMV-tdTomato-P2A-F3-Nedd4L) was designed and engineered according to our earlier protocol (20) and packaged into AAV9 (3.6 × 10^{13} vg/mL) by ViroVek Inc. Control AAV (pFB-CMV-tdTomato (1 × 10^{10} vg/mL) was purchased from Vector Biolabs. Mice older than 3 wk were first anesthetized under isoflurane and Ca$_V$-aβlator of low (1:3 dilution, final 9 × 10^{12} vg/mL, 20 μL volume, total 1.8 × 10^{11} vg) or high dose (final 3.6 × 10^{13} vg/mL, 20 μL volume, total 7.2 × 10^{11} vg) was subcutaneously injected into the left hind paw of the mouse from its ventral side with BD Insulin Syringes with BD Utra-Fine Needle. The needle was kept in the tissue for 1 to 2 min before being pulled out of the paw to minimize the potential leakage of the agent. No clear adverse effect of the Ca$_V$-aβlator on the mice was observed for both doses. For virus injection into mouse pups (P3 to P7), ice hypothermia and reduced volume (5 μL) were used for the plantar injection. Following injection, pups were kept on the heating pad until their body temperature returned to a normal level. The pups were then placed back into the cage in close vicinity to the mother.

Nerve Injury Model.
SNI of the sciatic nerve was performed in Thy1-GCaMP6s mice infected with Ca$_V$-aβlator from hind paw injection (62). In brief, mice were anesthetized with 3.5% isoflurane in air. Anesthesia was maintained with 1.2% isoflurane in air. A 0.5-cm-long incision in the left thigh was made to expose the sciatic nerve and its three branches. The common peroneal nerve and tibial nerve were ligated and axotomized by removing a 2- to 4-mm piece of each distal nerve stump. The sural nerve was kept intact.

In Vivo Ca^{2+} Imaging of DRG Neurons and Data Analysis.
Thy1-GCaMP6s mice were used for Ca^{2+} imaging of afferent sensory somas in the DRG. DRG window implantation was performed as described previously (32). In brief, mice were anesthetized with 100 mg/kg ketamine and 15 mg/kg xylazine. Following a 1-cm-long skin incision in the back between the L3 and L5 level of the spine, the muscles along the lateral aspects were detached and retracted. The long and short bracket of the vertebrae mount device was aligned with the left and right side of the L4 and L5 vertebrae, respectively, and registered with a locking screw. After the articular processes around the exposed DRG were trimmed, a thin layer of Kwik-Sil silicone elastomer was applied on top of DRG and a round coverslip was placed on top of the elastomer. The coverslip was secured to the vertebrae mount using cyanoacrylate and dental acrylic. Throughout the surgical procedure and recovery, the mouse body temperature was maintained at ~37 °C.

During imaging, awake mice were placed in a 2.9-cm-diameter transparent plastic cylinder mounted onto a heavy metal base to attenuate motion-related artifacts. Mice were habituated to this fixation device for at least 30 min before imaging. Imaging was performed using a Scientifica two-photon system equipped with a Ti:sapphire laser (Vision S, Coherent) tuned to 920 nm. The average laser power on the sample was ~20 to 30 mW. Images were collected at frame rates of 1.3 to 1.7 Hz at a resolution of 512 × 512 pixels using a 25× objective (numerical aperture = 1.05) immersed in artificial cerebrospinal fluid (aCSF) and with a 1× digital zoom. Image acquisition was performed using ScanImage software (Vidrio Technologies) and analyzed post hoc using ImageJ (NIH) and MATLAB (Mathworks) software.

Image analysis was performed as previously described with minor modifications (63). When the animal was quiet resting, motion artifacts in DRG imaging stacks were subtle and further corrected using the ImageJ stabilizer plugin. The active neurons were then extracted as individual components using custom code in MATLAB, and a temporal trace that captured their individual fluorescence intensity fluctuation was depicted. The neural activity deconvolution was further performed using sparse nonnegative deconvolution and implemented using the near-online OASIS algorithm (64, 65). The peak amplitude and number of spikes per min were analyzed. The $\Delta F/F_0$ was calculated as $\Delta F/F_0 = (F - F_0)/F_0 \times 100\%$, where F_0 is the baseline fluorescence signal corresponding to the inactive portions of the raw fluorescence trace during the 4-min recording. Average integrated Ca^{2+} activity was the average of $\Delta F/F$ over 4 min.

Behavior Tests.
Von Frey test. As an assay of mechanical sensitivity, we employed Dixon's up and down method to measure the animals' PWT (66). Mice were placed into transparent acrylic boxes (10 cm × 7 cm × 7 cm) over a mesh table and habituated for 30 min. A series of von Frey filaments (0.008, 0.02, 0.07, 0.16, 0.4, 0.6, 1.0, 1.4, 2.0, and 4.0 g) were then presented to the paw plantar surface in consecutive ascending order. In the absence of a paw-withdrawal response, the next stronger stimulus was presented; in the event of paw withdrawal, the next weaker stimulus was used. After the response threshold was first crossed, six data points were counted, at which time the two responses straddling the threshold were retrospectively designated as the first two responses of the series of 6. The 50% PWT was calculated as follows: 50% g threshold = (10[Xf +κδ])/10,000, where Xf = value (in log units) of the final von Frey hair used, κ = tabular value for the pattern of positive/negative responses (67), and δ = mean difference (in log units) between stimuli (here, 0.2699).

Thermal test. To measure the heat sensitivity, mice were individually placed in transparent acrylic boxes (10 cm × 7 cm × 7 cm) on the transparent glass pane of infrared plantar testing system (Model 37370, Ugo Basile) and habituated for 30 min. During the testing sessions, the lateral plantar aspect of the mouse hind paw was stimulated through the glass pane by a thermal emitter, which delivers calibrated radiant heat. The latency of significant paw withdrawal was scored automatically by the system. Each mouse was tested for 3 to 4 times at intervals of more than 1 h, and the mean was calculated as Hargreaves response.

Cold plate. Cold sensitivity was measured using a custom-built device assembled with a thermoelectric Peltier cold plate (CP-031; TE Technologies) and thermoelectric temperature controller (TC-720; TE Technologies). Before testing was performed, mice were individually placed in a transparent acrylic container placed on the plate and habituated for 30 min at room temperature. During testing, the temperature of plate was set at 0 °C and the withdrawal latencies were recorded. The withdrawal response was identified as hind paw lifting coupled with flinching.

Open field, rotarod, and locomotor function tests were assessed in tdTomato- and Ca_V-aβlator-injected mice without DRG window implantation and SNI surgery.

Open field test. Mice were allowed to run a 40-cm × 40-cm × 40-cm open field arena over a 10-min session (Stoelting). Video tracking for activity and anxiety was performed using ANY-maze software (Stoelting). Briefly, the distance traveled, time spent, and average speed in the center (a square area of 20 cm × 20 cm at the center of the arena) and at the periphery (band of 10 cm wide from the outer of the arena) of the arena were recorded and analyzed.

Rotarod test. An EZRod system with a test chamber (Omnitech Electronics) was used to perform the rotarod test. Mice were placed on a motorized rod, the rotation speed of which increased gradually from 0 to 100 rpm over a course of 3 min. The time in seconds each mouse spent on the accelerating rod before falling was recorded. For each mouse, rotarod performance was measured and averaged over 10 trials.

Locomotor function test. Three reflex tests were carried out as previously described (68). 1) Placing reflex: The mouse was held with the hind limbs slightly lower than the forelimbs, and the dorsal surfaces of the hind paws were brought into contact with the edge of a table. The experimenter recorded whether the hind paws were placed on the table surface reflexively. 2) Grasping reflex: The mouse was placed on a wire grid, and the experimenter recorded whether the hind paws grasped the wire on contact. 3) Righting reflex: The mouse was placed on its back on a flat surface, and the experimenter noted whether it immediately assumed the normal upright position. Scores for placing, grasping, and righting reflexes were based on counts of each normal reflex exhibited in five trials.

Cryosection. Four to six weeks following AAV injection into wild-type mice, they were euthanized for electrophysiology recording or cryosection imaging. The sciatic nerves, lumbar dorsal roots, DRGs, and ventral skin of the paws were collected and fixed in 4% paraformaldehyde for at least 2 h to overnight. Tissues were then washed in phosphate-buffered saline (PBS) three times, placed in 30% sucrose PBS overnight at 4 °C, and then embedded in the Tissue-Tek optimum cutting temperature solution (Sakura) within Tissue-Tek cryomolds. The cryomolds were then positioned on top of a thin layer of liquid 2-methylbutane within an aluminum foil boat, which was then placed over liquid nitrogen. Cryosections of 25 μm were obtained using a Leica CM1850 ultraviolet (UV) cryostat, and the sections were taken onto Superfrost slides (Fisherbrand). DAPI mounting medium (DAPI Fluoromount-G, SouthernBiotech) was directly applied on the sectioned tissues to make the tissues completely immersed in the medium, with coverslips placed over the medium. The medium was left dry for at least 2 h before a nail coat (Seche Vite dry fast top coat) was used to seal the side of the coverslips.

Confocal Imaging. Tissue cryosections were imaged using a Nikon Eclipse Ti A1-A laser scanning confocal microscope with NIS-Elements AR 5.02.00 64-bit software. Coherent OBIS 405, 488, and Sapphire 561 lasers and filter sets of 425 to 475 nm (blue channel), 500 to 550 nm (green channel), and 570 to 620 nm (red channel) were installed in the confocal system. Nikon Plan Apo 10×/0.45 DIC N1, VC 20×/0.75 DIC N2, and Plan Fluor 40×/1.30 Oil DIC H objectives were used. Image analysis was done with the Fiji ImageJ program. Because autofluorescence emitted by the organelles can be seen in both red and green channels, we used green autofluorescence for a background subtraction of red fluorescence signals to distinguish true tdTomato fluorescence from autofluorescence. Before subtraction for each image analysis, both red and green channel images were normalized with a 0.1% saturation setting unless specified.

DRG Culture Preparation. Following decapitation of the mice infected with AAV, lumbar DRGs from the AAV-injected side and the control side were harvested separately and transferred to Ca^{2+}-free, Mg^{2+}-free Hanks' balanced salt solution (HBSS; Invitrogen) containing the following (in mM): 137.9 NaCl, 5.3

KCl, 0.34 Na_2HPO_4, 0.44 K_2HPO_4, 5.6 glucose, 4.2 $NaHCO_3$, and 0.01% phenol red. Ganglia were treated with collagenase (1.5 mg/mL; Type P; Sigma-Aldrich) in HBSS for 20 min at 37 °C followed by 1× TrypLE (Thermo Fisher Scientific) for 2 min with gentle rotation. After the TrypLE was removed, the remaining TrypLE was neutralized with culture medium (modified Eagle's medium [MEM], with L-glutamine, Phenol Red, without sodium pyruvate; Thermo Fisher Scientific, #11095-080) supplemented with 10% horse serum (heat-inactivated; Invitrogen), 100 U/mL penicillin, 100 μg/mL streptomycin, MEM vitamin solution (Thermo Fisher Scientific), and B-27 supplement. The DRGs were left in the tubes vertically for 5 min and the serum-containing medium was decanted. DRGs were resuspended with serum-free MEM containing the supplements listed above and triturated using a fire-polished pasteur pipette. DRG neurons were plated on laminin-treated (0.05 mg/mL) glass coverslips, rinsed with 70% ethanol, and UV sterilized. Cultures were then incubated at 37 °C in 5% CO_2 and used for electrophysiological experiments at 24 to 48 h after plating.

Spinal Cord Slicing. The procedure for mouse spinal cord slicing was modified from published work (69, 70). In short, the spinal cord was first obtained through dissection of vertebrae from the mouse in 2 to 4 °C N-methyl-D-glucamine–4-(2-hydroxyethyl)-1-piperazineethanesulfonic acid (NMDG-Hepes) aCSF following its decapitation. NMDG-Hepes aCSF contains (in mM) 92 NMDG, 2.5 KCl, 1.25 NaH_2PO_4, 30 $NaHCO_3$, 20 Hepes, 25 glucose, 2 thiourea, 5 Na-ascorbate, 3 Na-pyruvate, 0.5 $CaCl_2$, and 10 $MgCl_2$, with the at pH 7.3 to 7.4 and osmolality measured and adjusted to 300 to 310 mOsmol/kg. The spinal cords were then placed into a small dish (2.5-cm diameter, 2-cm height) with a piece of filter paper at the bottom. The dish was quickly filled with 2% preheated low-melting-point agarose (Invitrogen Life Technologies) and placed on ice immediately to make the agarose solidify. The solidified agar blocks with embedded spinal cords were taken out from the small dish and placed in the slicing chamber of a Leica VT1200S vibrating blade microtome. The filter paper was removed, and transverse slices (350 μm) were cut using the microtome in 4 °C NMDG-Hepes aCSF. After all the slices were collected, they were transferred to a recovering solution in a chamber and kept in the NMDG-Hepes aCSF at 34 °C. A total of 2 M Na^+ spike-in solution (580 mg of NaCl dissolved in 5 mL of freshly prepared NMDG-Hepes aCSF) was prepared and added into the NMDG-Hepes aCSF at 34 °C every 5 min starting at the time of slice transfer at dilution ratios of 1:600, 1:600, 2:600, 4:600, and 8:600. Slices were transferred to Hepes holding aCSF after 25 min. Hepes holding aCSF contains (in mM) 92 NaCl, 2.5 KCl, 1.25 NaH_2PO_4, 30 $NaHCO_3$, 20 Hepes, 25 glucose, 2 thiourea, 5 Na-ascorbate, 3 Na-pyruvate, 2 $CaCl_2$, and 2 $MgCl_2$ and is titrated to pH 7.3 to 7.4. For mice older than 3 months old, there was a delay of 5 min for the addition of the Na^+ spike-in solution, and the slices were transferred from NMDG-Hepes aCSF to Hepes holding aCSF after 30 min.

Electrophysiology Recordings and Data Analysis. For cultured DRG neurons, whole-cell patch clamp recordings were performed using an EPC-10 patch clamp amplifier (HEKA Electronics) controlled by Pulse software (HEKA). Micropipettes were prepared from 1.5-mm thin-walled glass (World Precision Instruments) using a P97 microelectrode puller (Sutter Instruments). The internal solution contained (mM) the following: 135 cesium-methansulfonate (CsMESO3), 5 CsCl, 5 egtazic acid (EGTA), 1 MgCl2, 2 MgATP, and 10 Hepes (pH 7.3). The series resistance was typically between 1 and 2 MΩ. There was no electronic resistance compensation. The external solution contained (mM) 140 tetraethylammonium-MeSO3, 5 $BaCl_2$, and 10 Hepes (pH 7.4). Whole-cell I-V curves were generated from a family of step depolarizations (−60 mV to +80 mV from a holding potential of −90 mV). Currents were sampled at 20 kHz and filtered at 5 kHz. Traces were acquired at a repetition interval of 10 s. Leak and capacitive transients were subtracted using a P/4 protocol.

Dorsal horn neuron recordings from acute spinal cord slices are described (30, 69). In brief, voltage-clamp whole-cell patch recordings were used to record sEPSCs and sIPSCs from dorsal horn neurons in lamina I and II. Recordings were made at room temperature and the extracellular solution contained (in mM) 124 NaCl, 2.5 KCl, 1.25 NaH_2PO_4, 24 $NaHCO_3$, 12.5 glucose, 5 Hepes, 2 $CaCl_2$, and 1 $MgCl_2$ that was titrated to pH 7.3 to 7.4.

Recording electrodes (3 to 5 MΩ) were pulled from borosilicate glass capillaries (0.86-mm inner diameter, 1.5-mm outer diameter). The intracellular solution included the following (in mM): 120 Cs-methanesulfonate, 10

Na-methanesulfonate, 10 EGTA, 1 CaCl2, 10 Hepes, 5 lidocaine *N*-ethyl bromide quaternary salt Cl, 0.5 NaGTP, 5 MgATP, and 0.1% biocytin, with the pH adjusted to 7.2 with CsOH; osmolality was 280 mOsm/L. Cells were held at −70 mV and 0 mV for sEPSC and sIPSC recordings, respectively. Data were recorded and acquired using an Axopatch 200B amplifier and pClamp 9 software (Molecular Devices), filtered at 5 kHz, and digitized at 10 or 20 kHz. Lamina II appears translucent.

Mini Analysis software (Synaptosoft) was used for data analysis. For the analysis of sEPSCs and sIPSCs, their frequency, amplitude, rise time, decay τ (1/e = 63% decay time) and area under the curve were measured. Events thresholds were set to be 9 pA for sEPSCs and 8 pA for sIPSCs, which are close to three times of the root mean square (RMS) noise of the baseline.

Statistics. Prism software (GraphPad) was used to conduct the statistical analysis. Summary data are given as mean ± SEM when the samples followed a normal distribution and presented as median and 25 to 75% range when not they did not follow a normal distribution. Differences between two groups were assessed by unpaired two-tailed Student's *t* test when both groups of samples followed the Kolmogorov–Smirnov (KS) normality test. For data that failed normality testing, the two-tailed Mann–Whitney test was used. Grubb's test was used to remove outliers with $P < 0.01$ as significance. A multiple-group comparison was performed with one-way or two-way ANOVA when all groups of samples followed KS normality tests. Otherwise, the Kruskal–Wallis nonparametric test was used. Significance was set at $P < 0.05$.

Data Availability. All study data are included in the article and/or SI Appendix.

Author affiliations: [a]Department of Anesthesiology, Columbia University Medical Center, New York, NY 10032; [b]Department of Physiology and Cellular Biophysics, Columbia University Medical Center, New York, NY 10032; and [c]Department of Molecular Pharmacology and Therapeutics, Columbia University Medical Center, New York, NY 10032

1. C. Toth, J. Lander, S. Wiebe, The prevalence and impact of chronic pain with neuropathic pain symptoms in the general population. *Pain Med.* **10**, 918–929 (2009).
2. O. van Hecke, S. K. Austin, R. A. Khan, B. H. Smith, N. Torrance, Neuropathic pain in the general population: A systematic review of epidemiological studies. *Pain* **155**, 654–662 (2014).
3. L. Colloca et al., Neuropathic pain. *Nat. Rev. Dis. Primers* **3**, 17002 (2017).
4. D. Bates et al., A comprehensive algorithm for management of neuropathic pain. *Pain Med.* **20** (suppl. 1), S2–S12 (2019).
5. E. Cavalli, S. Mammana, F. Nicoletti, P. Bramanti, E. Mazzon, The neuropathic pain: An overview of the current treatment and future therapeutic approaches. *Int. J. Immunopathol. Pharmacol.* **33**, 2058738419838383 (2019).
6. A. Moore, S. Derry, P. Wiffen, Gabapentin for chronic neuropathic pain. *JAMA* **319**, 818–819 (2018).
7. J. Markman et al., Efficacy of pregabalin in post-traumatic peripheral neuropathic pain: A randomized, double-blind, placebo-controlled phase 3 trial. *J. Neurol.* **265**, 2815–2824 (2018).
8. B. Parsons, L. Tive, S. Huang, Gabapentin: A pooled analysis of adverse events from three clinical trials in patients with postherpetic neuralgia. *Am. J. Geriatr. Pharmacother.* **2**, 157–162 (2004).
9. Y. Yu et al., The efficacy of pregabalin for the management of acute and chronic postoperative pain in thoracotomy: A meta-analysis with trial sequential analysis of randomized-controlled trials. *J. Pain Res.* **12**, 159–170 (2018).
10. S. Atici et al., Liver and kidney toxicity in chronic use of opioids: An experimental long term treatment model. *J. Biosci.* **30**, 245–252 (2005).
11. D. J. Fink et al., Gene therapy for pain: Results of a phase I clinical trial. *Ann. Neurol.* **70**, 207–212 (2011).
12. C. Kibaly, H. H. Loh, P. Y. Law, A mechanistic approach to the development of gene therapy for chronic pain. *Int. Rev. Cell Mol. Biol.* **327**, 89–161 (2016).
13. N. S. Gee et al., The novel anticonvulsant drug, gabapentin (Neurontin), binds to the alpha2delta subunit of a calcium channel. *J. Biol. Chem.* **271**, 5768–5776 (1996).
14. M. J. Field et al., Identification of the alpha2-delta-1 subunit of voltage-dependent calcium channels as a molecular target for pain mediating the analgesic actions of pregabalin. *Proc. Natl. Acad. Sci. U.S.A.* **103**, 17537–17542 (2006).
15. A. Schmidtko, J. Lötsch, R. Freynhagen, G. Geisslinger, Ziconotide for treatment of severe chronic pain. *Lancet* **375**, 1569–1577 (2010).
16. J. Raingo, A. J. Castiglioni, D. Lipscombe, Alternative splicing controls G protein-dependent inhibition of N-type calcium channels in nociceptors. *Nat. Neurosci.* **10**, 285–292 (2007).
17. D. C. Yeomans et al., Decrease in inflammatory hyperalgesia by herpes vector-mediated knockdown of Nav1.7 sodium channels in primary afferents. *Hum. Gene Ther.* **16**, 271–277 (2005).
18. S. J. Kim et al., Effective relief of neuropathic pain by adeno-associated virus-mediated expression of a small hairpin RNA against GTP cyclohydrolase 1. *Mol. Pain* **5**, 67 (2009).
19. A. M. Moreno et al., Long-lasting analgesia via targeted in situ repression of Na$_V$1.7 in mice. *Sci. Transl. Med.* **13**, eaay9056 (2021).
20. T. J. Morgenstern, J. Park, Q. R. Fan, H. M. Colecraft, A potent voltage-gated calcium channel inhibitor engineered from a nanobody targeted to auxiliary Ca$_V$β subunits. *eLife* **8**, e49253 (2019).
21. M. Costigan, J. Scholz, C. J. Woolf, Neuropathic pain: A maladaptive response of the nervous system to damage. *Annu. Rev. Neurosci.* **32**, 1–32 (2009).
22. A. C. Dolphin, Calcium channel auxiliary α2δ and β subunits: Trafficking and one step beyond. *Nat. Rev. Neurosci.* **13**, 542–555 (2012).
23. E. L. Tran, L. K. Crawford, Revisiting PNS plasticity: How uninjured sensory afferents promote neuropathic pain. *Front. Cell. Neurosci.* **14**, 612982 (2020).
24. C. Peirs, R. P. Seal, Neural circuits for pain: Recent advances and current views. *Science* **354**, 578–584 (2016).
25. A. J. Todd, Neuronal circuitry for pain processing in the dorsal horn. *Nat. Rev. Neurosci.* **11**, 823–836 (2010).
26. Y. Mochizuki, M. K. Park, T. Mori, S. Kawashima, The difference in autofluorescence features of lipofuscin between brain and adrenal. *Zool. Sci.* **12**, 283–288 (1995).
27. C. W. Shuttleworth, Use of NAD(P)H and flavoprotein autofluorescence transients to probe neuron and astrocyte responses to synaptic activation. *Neurochem. Int.* **56**, 379–386 (2010).
28. H. Andersson, T. Baechi, M. Hoechl, C. Richter, Autofluorescence of living cells. *J. Microsc.* **191**, 1–7 (1998).
29. N. C. Whittington, S. Wray, Suppression of red blood cell autofluorescence for immunocytochemistry on fixed embryonic mouse tissue. *Curr. Protoc. Neurosci.* **81**, 2.28.1–2.28.12 (2017).
30. T. Takazawa et al., Inhibition mediated by glycinergic and GABAergic receptors on excitatory neurons in mouse superficial dorsal horn is location-specific but modified by inflammation. *J. Neurosci.* **37**, 2336–2348 (2017).
31. T. Takazawa, A. B. MacDermott, Glycinergic and GABAergic tonic inhibition fine tune inhibitory control in regionally distinct subpopulations of dorsal horn neurons. *J. Physiol.* **588**, 2571–2587 (2010).
32. C. Chen et al., Long-term imaging of dorsal root ganglia in awake behaving mice. *Nat. Commun.* **10**, 3087 (2019).
33. J. B. McCallum, W. M. Kwok, D. Sapunar, A. Fuchs, Q. H. Hogan, Painful peripheral nerve injury decreases calcium current in axotomized sensory neurons. *Anesthesiology* **105**, 160–168 (2006).
34. J. B. McCallum, H. E. Wu, Q. Tang, W. M. Kwok, Q. H. Hogan, Subtype-specific reduction of voltage-gated calcium current in medium-sized dorsal root ganglion neurons after painful peripheral nerve injury. *Neuroscience* **179**, 244–255 (2011).
35. S. S. Murali et al., High-voltage-activated calcium current subtypes in mouse DRG neurons adapt in a subpopulation-specific manner after nerve injury. *J. Neurophysiol.* **113**, 1511–1519 (2015).
36. Z. D. Luo et al., Upregulation of dorsal root ganglion (alpha)2(delta) calcium channel subunit and its correlation with allodynia in spinal nerve-injured rats. *J. Neurosci.* **21**, 1868–1875 (2001).
37. C. Y. Li, Y. H. Song, E. S. Higuera, Z. D. Luo, Spinal dorsal horn calcium channel alpha2delta-1 subunit upregulation contributes to peripheral nerve injury-induced tactile allodynia. *J. Neurosci.* **24**, 8494–8499 (2004).
38. C. S. Bauer et al., The increased trafficking of the calcium channel subunit alpha2delta-1 to presynaptic terminals in neuropathic pain is inhibited by the alpha2delta ligand pregabalin. *J. Neurosci.* **29**, 4076–4088 (2009).
39. S. Gao, X. Yao, N. Yan, Structure of human Ca$_V$2.2 channel blocked by the painkiller ziconotide. *Nature* **596**, 143–147 (2021).
40. J. R. Goss et al., Herpes vector-mediated expression of proenkephalin reduces bone cancer pain. *Ann. Neurol.* **52**, 662–665 (2002).
41. Z. Buraei, J. Yang, The ß subunit of voltage-gated Ca^{2+} channels. *Physiol. Rev.* **90**, 1461–1506 (2010).
42. R. Khanna et al., Targeting the CaVα-CaVβ interaction yields an antagonist of the N-type CaV2.2 channel with broad antinociceptive efficacy. *Pain* **160**, 1644–1661 (2019).
43. X. Chen et al., Small-molecule CaVα$_1$-CaVβ antagonist suppresses neuronal voltage-gated calcium-channel trafficking. *Proc. Natl. Acad. Sci. U.S.A.* **115**, E10566–E10575 (2018).
44. S. M. Garraway, Q. Xu, C. E. Inturrisi, siRNA-mediated knockdown of the NR1 subunit gene of the NMDA receptor attenuates formalin-induced pain behaviors in adult rats. *J. Pain* **10**, 380–390 (2009).
45. B. Hu et al., Therapeutic siRNA: State of the art. *Signal Transduct. Target. Ther.* **5**, 101 (2020).
46. N. D. Fagoe, R. Eggers, J. Verhaagen, M. R. Mason, A compact dual promoter adeno-associated viral vector for efficient delivery of two genes to dorsal root ganglion neurons. *Gene Ther.* **21**, 242–252 (2014).
47. T. Hirai et al., Intrathecal AAV serotype 9-mediated delivery of shRNA against TRPV1 attenuates thermal hyperalgesia in a mouse model of peripheral nerve injury. *Mol. Ther.* **22**, 409–419 (2014).
48. M. Glatzel et al., Adenoviral and adeno-associated viral transfer of genes to the peripheral nervous system. *Proc. Natl. Acad. Sci. U.S.A.* **97**, 442–447 (2000).
49. H. Yu et al., Intraganglionic AAV6 results in efficient and long-term gene transfer to peripheral sensory nervous system in adult rats. *PLoS One* **8**, e61266 (2013).
50. Y. Huang et al., Development of viral vectors for gene therapy for chronic pain. *Pain Res. Treat.* **2011**, 968218 (2011).
51. C. Peirs, R. Dallel, A. J. Todd, Recent advances in our understanding of the organization of dorsal horn neuron populations and their contribution to cutaneous mechanical allodynia. *J. Neural Transm. (Vienna)* **127**, 505–525 (2020).
52. K. Y. Lee, S. Ratté, S. A. Prescott, Excitatory neurons are more disinhibited than inhibitory neurons by chloride dysregulation in the spinal dorsal horn. *eLife* **8**, e49753 (2019).
53. R. Bardoni et al., Pre- and postsynaptic inhibitory control in the spinal cord dorsal horn. *Ann. N. Y. Acad. Sci.* **1279**, 90–96 (2013).
54. J. Braz, C. Solorzano, X. Wang, A. I. Basbaum, Transmitting pain and itch messages: A contemporary view of the spinal cord circuits that generate gate control. *Neuron* **82**, 522–536 (2014).
55. P. Inquimbert et al., NMDA receptor activation underlies the loss of spinal dorsal horn neurons and the transition to persistent pain after peripheral nerve injury. *Cell Rep.* **23**, 2678–2689 (2018).
56. A. Etlin et al., Functional synaptic integration of forebrain GABAergic precursors into the adult spinal cord. *J. Neurosci.* **36**, 11634–11645 (2016).

57. I. J. Llewellyn-Smith, A. I. Basbaum, J. M. Bráz, Long-term, dynamic synaptic reorganization after GABAergic precursor cell transplantation into adult mouse spinal cord. *J. Comp. Neurol.* **526**, 480–495 (2018).
58. S. Møiniche, H. Kehlet, J. B. Dahl, A qualitative and quantitative systematic review of preemptive analgesia for postoperative pain relief: The role of timing of analgesia. *Anesthesiology* **96**, 725–741 (2002).
59. J. Katz, Pre-emptive analgesia: Importance of timing. *Can. J. Anaesth.* **48**, 105–114 (2001).
60. B. M. Muehling *et al.*, Reduction of postoperative pulmonary complications after lung surgery using a fast track clinical pathway. *Eur. J. Cardiothorac. Surg.* **34**, 174–180 (2008).
61. J. Cichon *et al.*, Imaging neuronal activity in the central and peripheral nervous systems using new Thy1.2-GCaMP6 transgenic mouse lines. *J. Neurosci. Methods* **334**, 108535 (2020).
62. I. Decosterd, C. J. Woolf, Spared nerve injury: An animal model of persistent peripheral neuropathic pain. *Pain* **87**, 149–158 (2000).
63. A. Adler, R. Zhao, M. E. Shin, R. Yasuda, W. B. Gan, Somatostatin-expressing interneurons enable and maintain learning-dependent sequential activation of pyramidal neurons. *Neuron* **102**, 202–216.e7 (2019).
64. J. Friedrich, P. Zhou, L. Paninski, Fast online deconvolution of calcium imaging data. *PLOS Comput. Biol.* **13**, e1005423 (2017).
65. A. Giovannucci *et al.*, CaImAn an open source tool for scalable calcium imaging data analysis. *eLife* **8**, e38173 (2019).
66. W. J. Dixon, Efficient analysis of experimental observations. *Annu. Rev. Pharmacol. Toxicol.* **20**, 441–462 (1980).
67. S. R. Chaplan, F. W. Bach, J. W. Pogrel, J. M. Chung, T. L. Yaksh, Quantitative assessment of tactile allodynia in the rat paw. *J. Neurosci. Methods* **53**, 55–63 (1994).
68. L. Sun *et al.*, Contribution of DNMT1 to neuropathic pain genesis partially through epigenetically repressing *Kcna2* in primary afferent neurons. *J. Neurosci.* **39**, 6595–6607 (2019).
69. C. K. Tong, A. B. MacDermott, Synaptic GluN2A and GluN2B containing NMDA receptors within the superficial dorsal horn activated following primary afferent stimulation. *J. Neurosci.* **34**, 10808–10820 (2014).
70. J. T. Ting *et al.*, Preparation of acute brain slices using an optimized N-methyl-D-glucamine protective recovery method. *J. Vis. Exp.* **132**, 53825 (2018).